Catalytic Activation of Activated Carbon Fibers via Palladium Aerosol Nanoparticles for Use in Electroless Silver Deposition

Jeong Hoon Byeon,[†] Byung Ju Ko,[‡] and Jungho Hwang*[,†]

School of Mechanical Engineering, Yonsei University, Seoul 120-749, and Corporate R & D Division, Hyundai Motors Company, Wanju 565-703, Republic of Korea

Received: November 13, 2007; In Final Form: December 7, 2007

A method of catalytic activation with palladium aerosol nanoparticles produced by spark generation was introduced. These catalytic particles were deposited onto the surfaces of activated carbon fibers (ACFs). After thermal curing, the catalytically activated ACFs were placed into a solution for electroless deposition (ELD) of silver. Homogeneous silver coatings on ACFs were achieved under various activation intensities and ELD times, and the results were compared to those obtained with a conventional "two-step" activation. Morphological, chemical, and textural properties of both catalytically activated ACFs and electroless silver deposited ACFs were characterized. When the activation intensity increased from 0.23 to 4.25 mg/g (palladium/ACFs) for an ELD time of 10 min, our aerosol activation increased the silver deposition from 7.1 to 13.2 mg/g (silver/ACFs) and the average size of the silver particles from 4.9 to 38.8 nm. However, the surface area and pore volume of the ACFs decreased from 1382 to 1286 m^2/g and from 0.77 to 0.67 cm^3/g, respectively.

Introduction

Porous carbon materials, due to their extensive specific surface area, high adsorption capacity, microstructure, and special surface reactivity, have been widely used in separation, purification, and catalytic processes.[1,2] Activated carbon fibers (ACFs), highly microporous carbon materials,[3−5] are commercially available in the form of fiber tows, cloths (fabrics), papers, mats, and felts.[6] ACFs have a larger micropore volume and a more uniform micropore size distribution than granular activated carbons (GACs) and, thus, are considered to have a larger adsorption capacity and greater adsorption and desorption rates.[7−12] The ACFs may be packed or constructed to fit almost any geometry for almost any catalytic application and satisfy the requirements of high catalyst effectiveness and a low pressure drop for finely divided catalysts, but avoid the technical problems associated with powders.

The electroless deposition (ELD) of metal is a simple chemical process for depositing metal layers onto nonconductive or conductive materials with complicated configurations that are widely used in the automotive, aerospace, packaging, appliance, optics, and electronics industries.[13−16] The initiation of the ELD process is preceded by a surface activation to provide catalytic sites on the material surface. However, conventional activations require a long process time and intermittent water rinsing and drying, involve the loss of expensive metal ions, and create environmental pollution problems.[17] Consequently, it is highly desirable to develop simple and more economically and ecologically attractive activations prior to the ELD process.[13,15,17] Many researchers have investigated methods to advance the activation using laser,[18] ultraviolet (UV) laser or UV/VUV (vacuum ultraviolet) excimer lamps,[19] plasma,[20] and ion beams.[21] However, these techniques require specialized conditions such as vacuum and the coating of palladium (Pd) compounds using spinning-on, spraying, or dip coating.[19,22,23] To improve the catalytic surface activation, recently, Byeon et al.[24] reported a strategy for site-selective catalytic surface activation via platinum aerosol nanoparticles for use in silver micropatterning. Aerosol catalysis is shown to be a powerful tool for investigating the catalytic properties of freshly formed nanoparticles in situ and without substrate interference.[25]

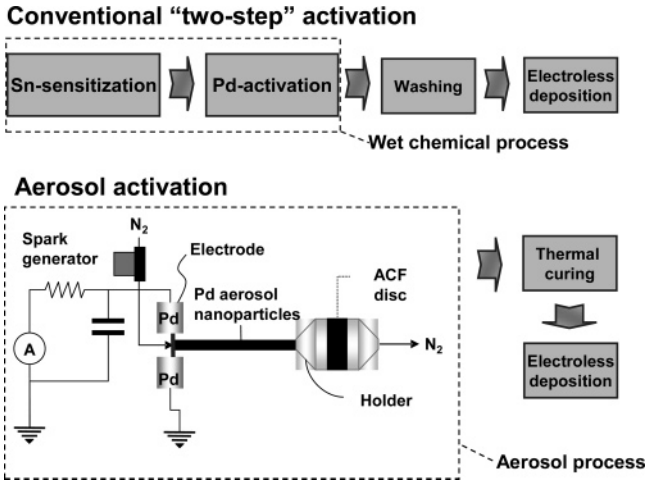

Figure 1. Procedures of conventional and aerosol activation.

This paper introduces a strategy for catalytic surface activation by the production of Pd aerosol nanoparticles via spark generation (Figure 1). Our aerosol activation involves fewer steps than conventional surface activation and does not require wet chemical steps. Spark generation has been used to produce the particles of metals, alloys, and compounds for a wide range of materials with particle sizes ranging from several nanometers up to ∼100 μm.[26] In this study, spark-generated nanoparticles were captured by ACFs due to fibrous filtration.[27] After thermal curing, the ACFs that were catalytically activated by the Pd nanoparticles were immersed in a silver ELD solution to form

* To whom correspondence should be addressed. E-mail: hwangjh@yonsei.ac.kr. Phone: (+82-2) 2123-2821. Fax: (+82-2) 312-2821.
[†] Yonsei University.
[‡] Hyundai Motors Co.

10.1021/jp7108225 CCC: $40.75
Published on Web 02/19/2008

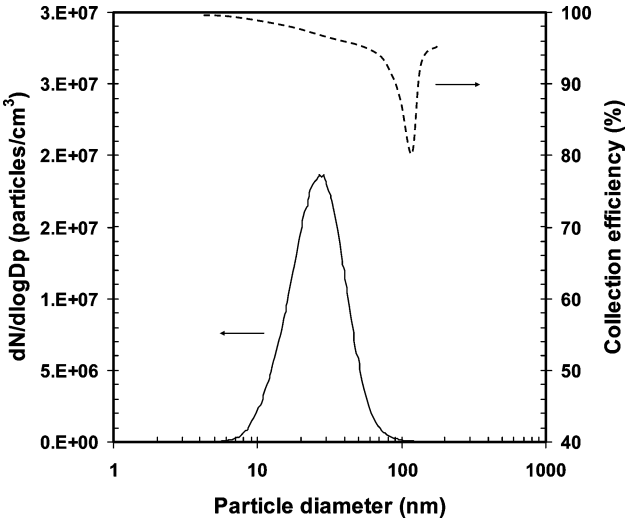

Figure 2. Particle size distribution of spark-generated aerosol nanoparticles and collection efficiency of ACFs.

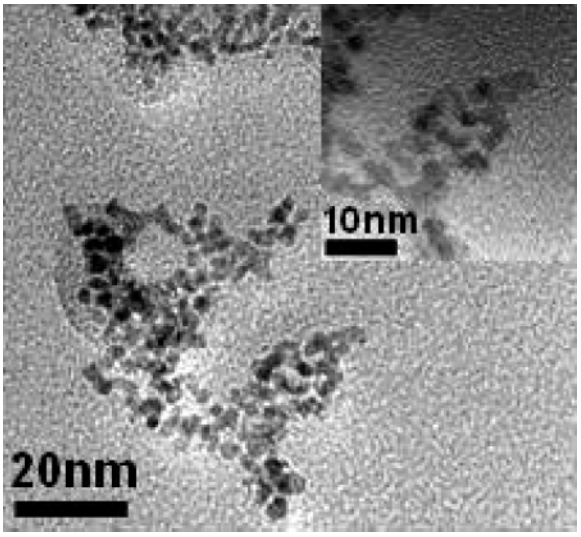

Figure 3. HRTEM micrograph of spark-generated nanoparticles.

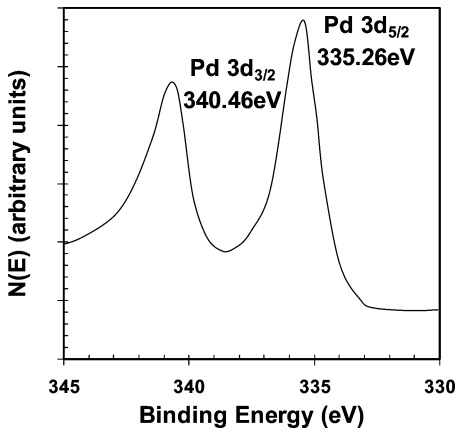

Figure 4. XPS profile of spark-generated aerosol nanoparticles.

a silver layer on the activated ACFs, and the reduction−oxidation reactions occurred preferentially around the Pd nanoparticles.

Experimental Section

Our catalytic surface activation involved the spark generation of Pd aerosol nanoparticles and their filtration by rayon-based ACFs (38 mm in diameter and 2.6 mm in thickness, KF-1600, Toyobo). A spark was generated between two identical Pd rods (diameter 3 mm, length 100 mm, Nilaco, Japan) inside a reactor (volume 42.8 cm^3) under a pure nitrogen environment (less than 10^{-4} impurities) at STP.[24,28] The flow rate of the nitrogen gas, which was controlled by a mass flow controller, was set to 2 L/min. The electrical circuit specifications were as follows: resistance of 0.5 MΩ, capacitance of 10 nF, loading current of 2 mA, applied voltage of 3 kV, and frequency of 667 Hz. The gas temperature inside the spark channel was increased beyond a critical value,[29] which was sufficient to sublimate parts of the electrodes. Since the duration of each spark was very short (∼1.5 ms) and the vapors were rapidly cooled after the spark was generated, supersaturation was achieved and the nanoparticles were formed by nucleation/condensation. To prevent the detachment of the nanoparticles from the surface of the ACF, the ACF was separated from the holder and cured in air at 190 °C for 5 min.

For comparison purposes, the surface of another ACF was activated by a conventional "two-step" process (Figure 1), which requires sensitization. The ACF was first sensitized by immersing it in an aqueous solution containing $SnCl_2$, HCl (0.05 mL), and deionized (DI) water (49.95 mL) for 2 min, followed by rinsing with DI water. The subsequent activation was carried out in a $PdCl_2$ solution of $PdCl_2$, HCl (0.05 mL), and DI water (49.95 mL) for 2 min, followed by rinsing again with DI water. The amounts of $SnCl_2$ and $PdCl_2$ in each aqueous solution were varied between 2 and 36 mg and between 1 and 18 mg, respectively.

Once the ACFs were activated by our aerosol process or the conventional process, the ACFs were immersed in a silver ELD solution for the deposition of silver onto the surfaces of the activated ACFs. Reactions of silver deposition were initiated by the reaction of hydrazine with hydroxide ions, producing nitrogen gas and water with a simultaneous release of electrons. The electrons were transferred across the Pd island and used for the decomposition of Ag−amine complexes into Ag metals, generating ammonia gas as a byproduct. Nitrogen and ammonia gases evolved as bubbles during the ELD process. The ACFs were vigorously rinsed with DI water after the ELD to remove the residual and then set aside to be dried. Two solutions were mixed and used for the ELD solution. Solution A contained 1 g of $AgNO_3$, 60 g of Na_2EDTA, 88 mL of isopropyl alcohol, 12 mL of acetic acid, and 400 mL of NH_4OH in 1 L of DI water. Solution B contained 3 mL of hydrazine, 2 mL of mercerine, and 400 mL of ethyl alcohol in 1 L of DI water. A 50 mL portion of solution A and 30 mL of solution B were mixed together, and the activated ACFs were then immersed into this mixture for 2−30 min at 20 °C so that the silver particles would be deposited on the activated ACFs.

The size distribution of Pd aerosol nanoparticles was measured by a scanning mobility particle sizer (SMPS) system comprising an electrostatic classifier (TSI 3085), ultrafine condensation particle counter (TSI 3025), and aerosol charge neutralizer. The SMPS system, which measures the mobility equivalent diameter, was operated at a sample flow of 0.3 L/min, sheath flow of 3 L/min, and scan time of 180 s (measurement range 4.61−157 nm). The number concentration of the particles that penetrated through the ACFs was also measured with the SMPS system. After the particles were sampled on a porous carbon-supported copper grid positioned on a polyamide membrane filter located 20 cm downstream of the spark generator, the morphologies and microstructures of the Pd nanoparticles were analyzed using high-resolution transmission electron microscopy (HRTEM; JEM-3010) operated at 300 kV.

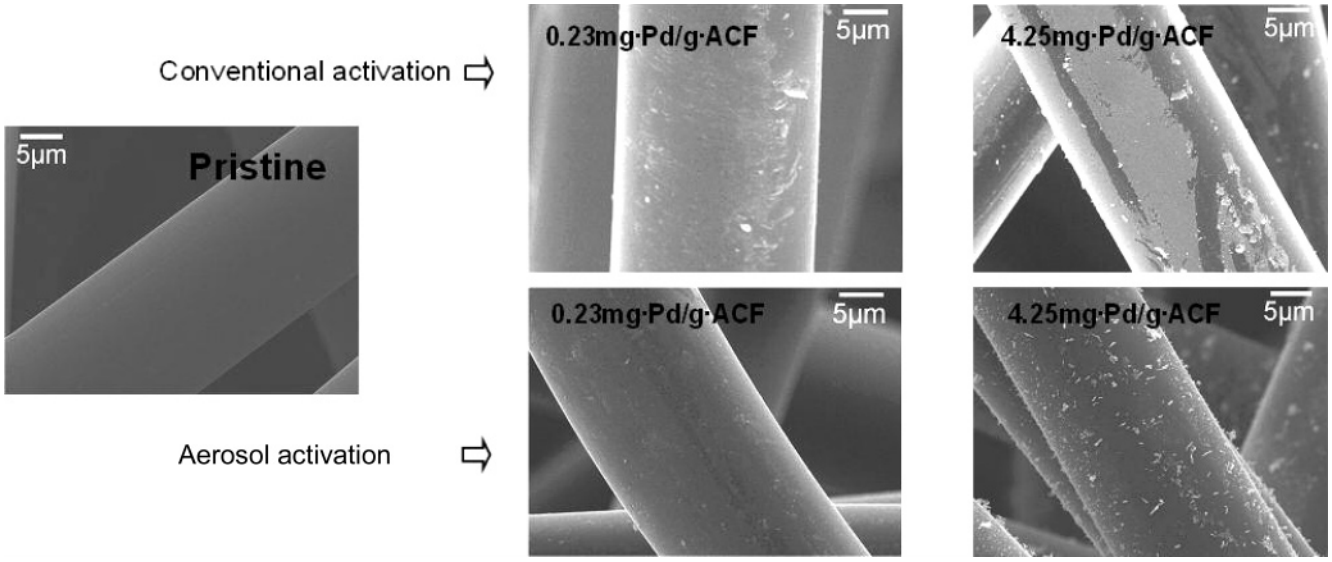

Figure 5. SEM micrographs of conventionally activated and aerosol-activated ACFs.

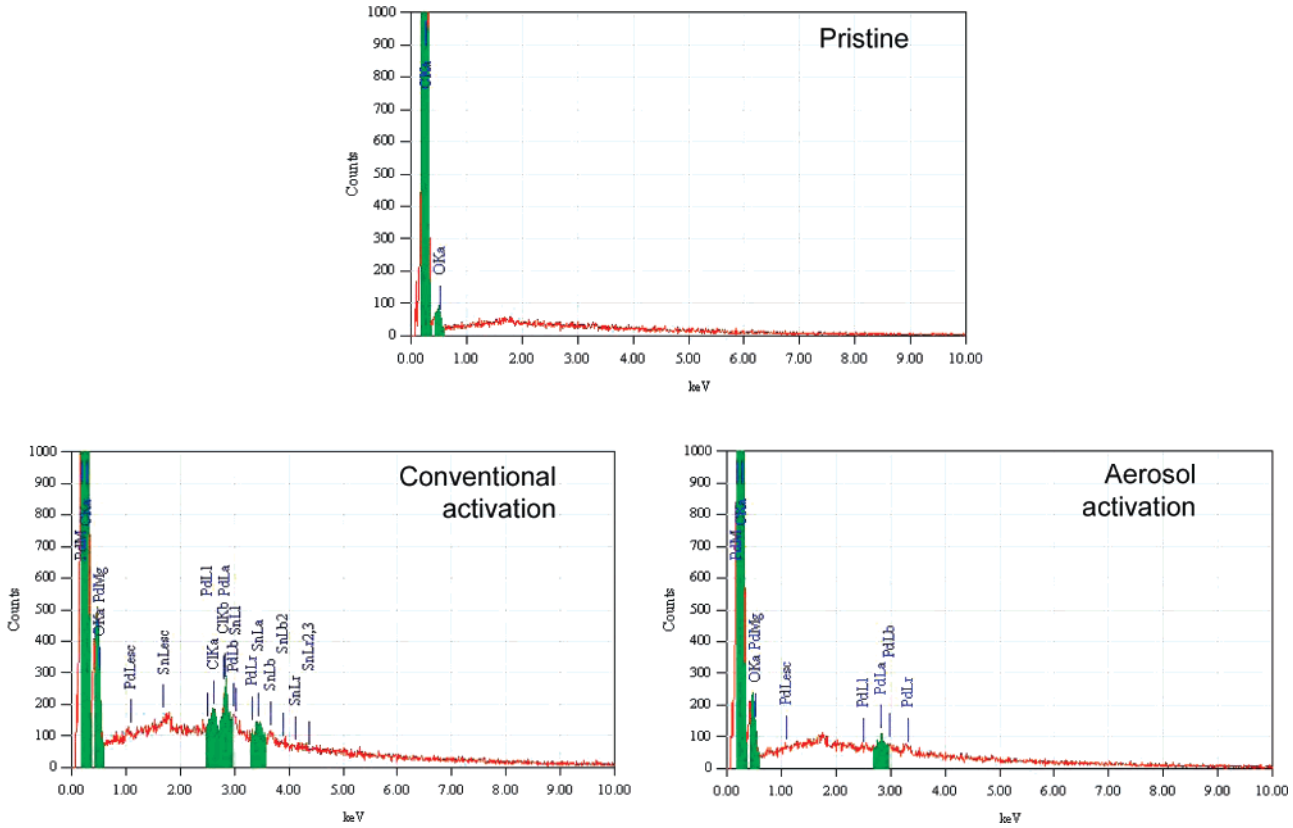

Figure 6. EDX profiles of conventionally activated and aerosol-activated ACFs.

X-ray photoelectron spectroscopy (XPS) measurements were performed on a Kratos Axis HIS spectrometer using a monochromatized Al Kα X-ray source (1486.6 eV photons) at a constant dwell time of 100 ms and pass energy of 40 eV. The X-ray source was run at a power of 150 W (15 kV and 10 mA). The pressure in the analysis chamber was maintained under 10^{-8} Torr during the measurements. All binding energies (BEs) were referenced to the C 1s hydrocarbon peak at 284.6 eV. Field-emission scanning electron microscopy (FESEM; JSM-6500F, JEOL, Japan) images and energy dispersive X-ray (EDX; JED-2300, JEOL, Japan) profiles were obtained at an accelerating voltage of 15 kV. The amount of silver particles deposited on the ACFs was determined by inductively coupled plasma atomic emission spectroscopy (ICP-AES; Elan 6000, Perkin-Elmer). Approximately 0.1 g of the sample was dissolved in 50 mL of nitric acid, and the mixture was diluted to 100 mL with DI water. After 3 h, the sample was filtered out, and a part of the remaining mixture was delivered in a volumetric flask for ICP-AES analyses. X-ray diffraction (XRD) studies of the silver particles were carried out on a Rigaku RINT-2100 diffractometer equipped with a thin-film attachment using Cu $K\alpha$ radiation (40 kV, 40 mA). The 2θ angles ranged from 10° to 90° at 4°/min by step scanning at an interval of 0.08°. The crystallite size of silver was calculated from the XRD spectra in accordance with Scherrer's formula ($t = 0.9\lambda/(B \cos \theta)$). Nitrogen adsorption isotherms of the ACF samples were measured using a

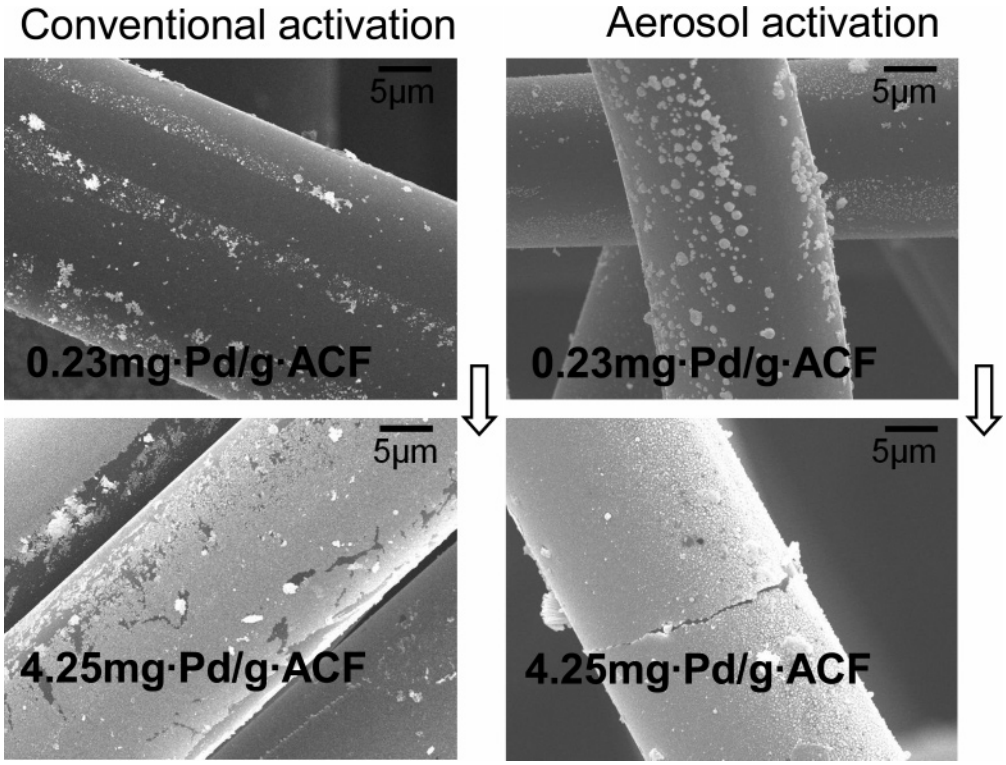

Figure 7. SEM micrographs of particle-deposited ACFs vs activation intensity.

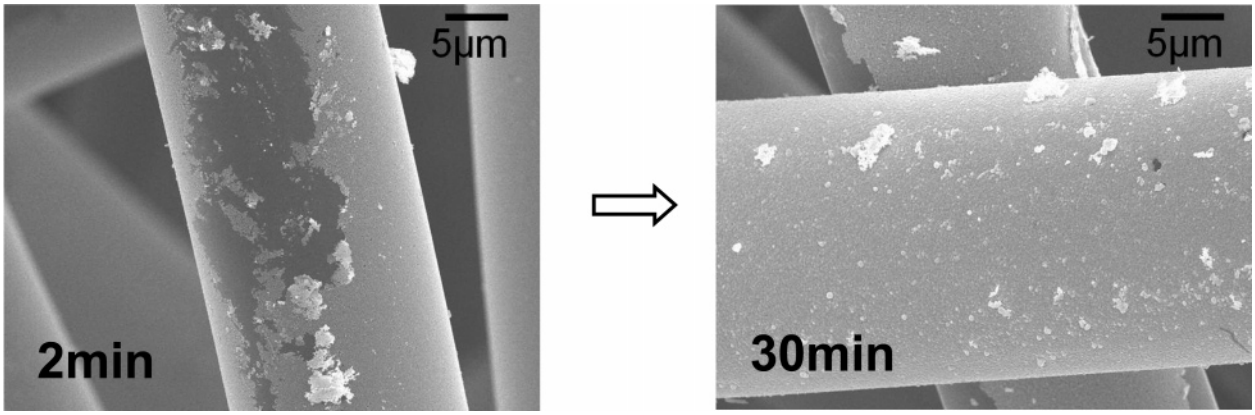

Figure 8. SEM micrographs of particle-deposited ACFs vs ELD time.

porosimeter (ASAP 2010, Micromeritics Ins. Corp.) at 77.4 K with relative pressure ranging from 10^{-6} to 1. High-purity (99.9999%) nitrogen was used for a material to be adsorbed. All the samples were degassed at 573 K for 2 h before each measurement. The specific surface area was determined using the BET equation. The total pore volume, which was estimated on the basis of the N_2 volume adsorbed at a relative saturation pressure (~0.996), actually corresponded to the total amount adsorbed. The pore size distribution was determined using the BJH (Barrett, Joyner, and Halenda) method, which uses the area of the pore walls and the Kelvin equation to correlate the relative N_2 pressure at equilibrium with the amount of porous solid with the size of the pores where the capillary condensation occurs.

Results and Discussion

Figure 2 shows the size distribution of spark-generated aerosol nanoparticles measured using the SMPS system. The geometric mean diameter and geometric standard deviation were 25.5 nm and 1.54, respectively. The total number concentration was 8.8 $\times$ 10^6 particles/cm^3. Figure 2 also shows the fractional (grade) collection efficiency of ACFs as a function of particle size. The efficiency is defined by

$$\eta_{ACF}(d_p) = 1 - [C_{ACF}(d_p)/C_0(d_p)] \quad (1)$$

where $C_0(d_p)$ is the free-stream concentration of the particles and $C_{ACF}(d_p)$ is the concentration after filtration by the ACFs. The morphology and structure of the nanoparticles were characterized by HRTEM and XPS, respectively. The HRTEM micrograph (Figure 3) shows that the nanoparticles were agglomerates of primary particles (each ~28 Å in diameter). The XPS profile (Figure 4) of the nanoparticles reveals that they were pure Pd. The BE doublets with the BEs of the Pd $3d_{5/2}$ and Pd $3d_{3/2}$ peak components located at approximately 335 and 340 eV, respectively, are assigned to the Pd^0 species.[30] Figure 5 shows SEM micrographs of conventionally activated and aerosol-activated ACFs. While pristine ACFs had a clean

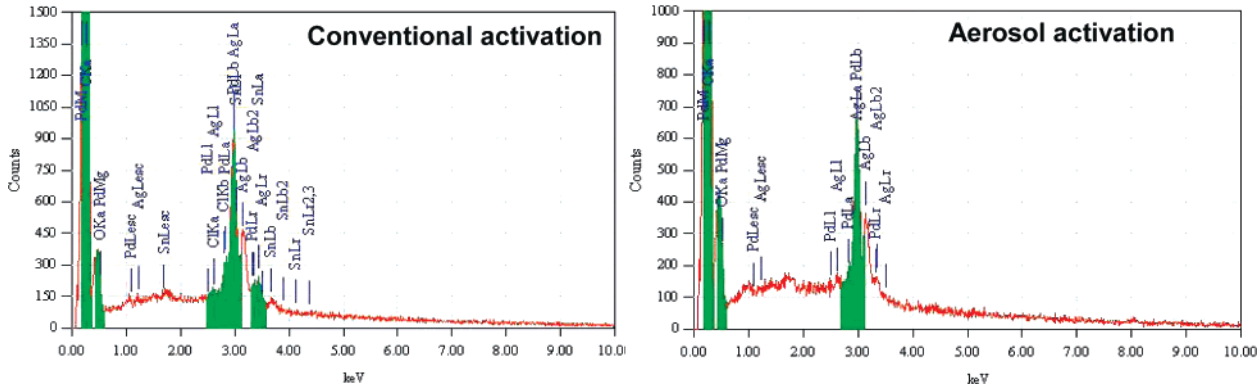

Figure 9. EDX profiles of particle-deposited ACFs (10 min of ELD, 1.42 mg of Pd/g of ACF).

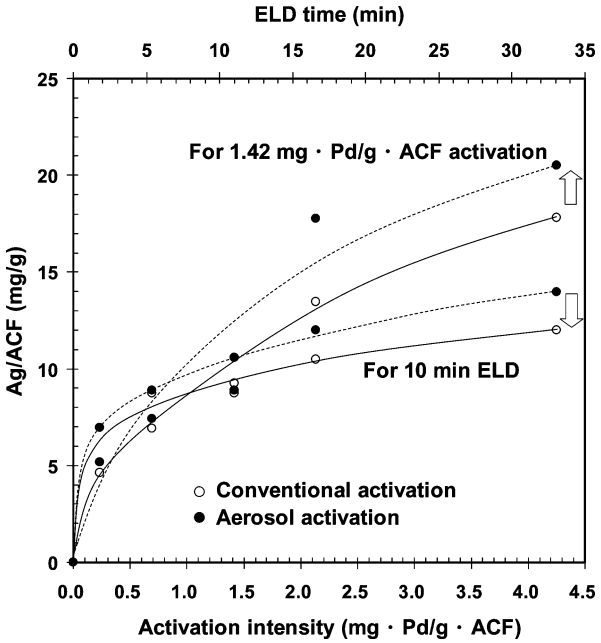

Figure 10. Results of ICP-AES analyses of silver-deposited ACFs.

TABLE 1: Crystal Sizes (nm) of Silver Particles vs Activation Intensity and ELD Time

ELD time (min)	0.23 mg of Pd/g of ACFs		0.69 mg of Pd/g of ACFs		1.42 mg of Pd/g of ACFs		4.25 mg of Pd/g of ACFs	
	CA[a]	AA[b]	CA	AA	CA	AA	CA	AA
2	2.21	3.48	7.01	10.78	12.04	13.89	26.63	28.84
5	3.55	4.21	9.33	10.02	17.12	19.51	31.11	32.89
10	4.22	4.93	11.36	12.02	20.33	22.65	35.14	38.79
18	5.01	5.28	14.88	15.68	23.25	26.01	39.18	41.24
30	5.66	6.13	16.16	16.81	31.05	33.25	46.13	48.21

[a] Conventional activation. [b] Aerosol activation.

surface, in any activation, more particles were deposited on the ACFs by increasing the activation intensity from 0.23 to 4.25 mg of Pd/g of ACFs. From the EDX analyses (Figure 6), it was found that the pristine sample contained carbon and oxygen, which may have originated from the ACFs, while any activated sample contained a small amount of Pd. The conventionally activated sample also contained a small amount of tin and chlorine, which may have originated from tin sensitization and Pd activation.

Figure 7 shows that particles on the ACFs were subsequently formed after the ELD process. The SEM micrographs of conventional and aerosol activations were obtained by varying

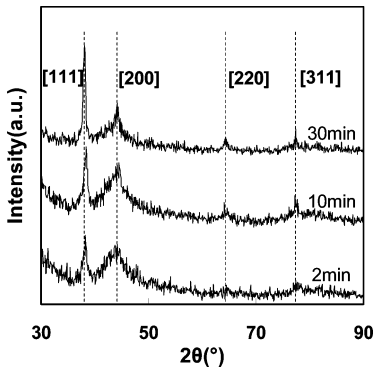

Figure 11. Results of XRD analyses of silver-deposited ACFs.

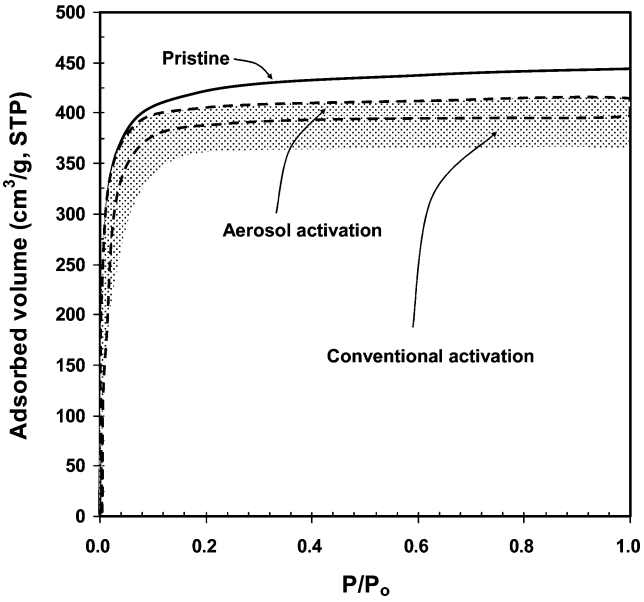

Figure 12. Adsorption isotherms of silver-deposited ACFs.

the activation intensity obtained after ELD for 10 min. The amount of particles was proportional to the activation intensity. Figure 8 shows the trend of particle deposition on aerosol-activated ACFs with ELD time at an activation intensity of 1.42 mg of Pd/g of ACFs. From the EDX analyses (Figure 9), it was found that the coated metal was mainly comprised of silver; however, it contained a small amount of Pd. Carbon and oxygen, which may have originated from the ACFs, were also detected. For the conventionally activated ACF, tin and chlorine were detected in addition to silver, Pd, carbon, and oxygen. Figure

TABLE 2: Textural Properties of Silver-Deposited ACFs vs Activation Intensity and ELD Time

ELD time (min)	TSSA[a]/MSSA[b]/TPV[c]/MPV[d]/APD[e] (1610/1593/0.87/0.85/17.7 for pristine)			
	0.23 mg of Pd/g of ACFs		4.25 mg of Pd/g of ACFs	
	CA	AA	CA	AA
2	1399/1226/0.72/0.70/17.0	1532/1488/0.80/0.78/17.5	1277/1202/0.65/0.64/16.8	1359/1325/0.72/0.70/17.1
10	1242/1206/0.69/0.67/16.5	1382/1358/0.77/0.76/17.2	1104/1072/0.60/0.57/16.3	1286/1225/0.67/0.65/16.9
30	1091/1003/0.65/0.62/15.9	1284/1236/0.69/0.67/16.6	912/803/0.52/0.51/15.4	1201/1056/0.61/0.59/16.1

[a] Total specific surface area (m^2/g). [b] Micropore specific surface area (m^2/g). [c] Total pore volume (cm^3/g). [d] Micropore volume (cm^3/g). [e] Average pore diameter (Å).

10 summarizes the plots of the mass of silver deposited onto the ACFs as a function of the activation intensity (for an ELD time of 10 min) and ELD time (at an activation intensity of 1.42 mg of Pd/g of ACFs). The results were obtained from the ICP-AES analyses. The mass increased with time due to a continuous reduction in silver ions on previously deposited silver particles (autocatalytic process).[14,22] The XRD profiles (Figure 11) of the silver particles show that there exist four peaks located at $2\theta = 38.2°$, 44.4°, 54.5°, and 77.5°. A comparison of these peaks with the data from powder diffraction file no. 01-0783 reveals that these peaks correspond to the [111], [200], [220], and [311] planes of the face-centered cubic phase of silver. The data imply the characteristics of pure metallic silver with good crystallinity and without any impurity phase. The intensities of the silver peaks increased with increasing ELD time (or activation intensity), which was caused by the growth of the silver particles. The average crystal sizes were evaluated according to Scherrer's formula, and the results are shown in Table 1. It was found that the size was proportional to either the activation intensity or the ELD time.

Figure 12 shows that a major uptake occurred at a relatively low pressure ($P/P_o < 1$) and a plateau was attained at $P/P_o \approx 0.3$, implying that all the ACF samples had microporous characteristics (type I isotherm) according to the IUPAC classification.[31] The specific surface area of the pristine ACFs was the largest; however, it decreased as the amount of deposited silver increased since the deposited silver particles could block or occupy some pores of the pristine ACFs. Detailed results of the textural properties of the samples are summarized in Table 2. When either the activation intensity or ELD time was increased in our aerosol activation, the decrease in the specific surface areas, pore volumes, and average pore diameters was less than that in the conventional activation.

Conclusions

Using our aerosol activation and ELD, it was possible to create stable metal layers on ACFs. When the activation intensity increased from 0.23 to 4.25 mg/g (palladium/ACFs) for an ELD time of 10 min, our aerosol activation increased the silver deposition from 7.1 to 13.2 mg/g (silver/ACFs) and the average size of the silver particles from 4.9 to 38.8 nm. However, the surface area and pore volume of the ACFs decreased from 1382 to 1286 m^2/g and from 0.77 to 0.67 cm^3/g, respectively. Our aerosol activation method can be applied to activate porous carbon objects of different thicknesses with the appropriate selection of flow direction, flow velocity, and number of sparks generated.

Acknowledgment. This study has been supported by a Korea Institute of Environmental Science and Technology (KIEST) grant (013-071-052).

References and Notes

(1) Tang, S.; Lu, N.; Wang, J. K.; Ryu, S.-K.; Choi, H.-S. *J. Phys. Chem. C* **2007**, *111*, 1820.
(2) Byeon, J. H.; Yoon, K. Y.; Park, J. H.; Hwang, J. *Carbon* **2007**, *45*, 2313.
(3) Yang, C. M.; Kaneko, K. *J. Colloid Interface Sci.* **2002**, *246*, 34.
(4) Moon, J. S.; Park, K. K.; Kim, J. H.; Seo, G. *Appl. Catal., A* **2000**, *201*, 81.
(5) Chen, S.; Zeng, H. *Carbon* **2003**, *41*, 1265.
(6) Matatov-Meytal, Y.; Sheintuch, M. *Appl. Catal., A* **2002**, *231*, 1.
(7) Shen, W.; Guo, Q.; Zhang, Y.; Liu, Y.; Zheng, J.; Cheng, J.; Fan, J. *Colloids Surf., A* **2006**, *273*, 147.
(8) Fu, P.; Luan, Y.; Dai, X. *J. Mol. Catal. A* **2004**, *221*, 81.
(9) Park, S. H.; Kim, C.; Jeong, Y. I.; Lim, D. Y.; Lee, Y. E.; Yang, K. S. *Synth. Met.* **2004**, *146*, 207.
(10) Li, C. Y.; Wan, Y. Z.; Wang, J.; Wang, Y. L.; Jiang, X. Q.; Han, L. M. *Carbon* **1998**, *36*, 61.
(11) Mochida, I.; Korai, Y.; Shirahama, M.; Kawano, S.; Hada, T.; Seo, Y.; Yoshikawa, M.; Yasutake, A. *Carbon* **2000**, *38*, 227.
(12) Vilaplana-Ortego, E.; Alcaiz-Monge, J.; Cazorla-Amorós, D.; Linares-Solano, A. *Fuel Process. Technol.* **2002**, *77*−*78*, 445.
(13) Prissanaroon, W.; Brack, N.; Pigram, P. J.; Hale, P.; Kappen, P.; Liesegang, J. *Thin Solid Films* **2005**, *477*, 131.
(14) Schaefers, S.; Rast, L.; Stanishevsky, A. *Mater. Lett.* **2006**, *60*, 706.
(15) Šimor, M.; Ráhel, J.; Černák, M.; Imahori, Y.; Štefečka, M.; Kando, M. *Surf. Coat. Technol.* **2003**, *172*, 1.
(16) Metz, K. M.; Divya, D.; Hamers, R. J. *J. Phys. Chem. C* **2007**, *111*, 7260.
(17) Touchais-Papet, E.; Charbonnier, M.; Romand, M. *Appl. Surf. Sci.* **1999**, *138*−*139*, 557.
(18) Chen, D.; Lu, Q.; Zhao, Y. *Appl. Surf. Sci.* **2006**, *253*, 1573.
(19) Esrom, H. *Appl. Surf. Sci.* **2000**, *168*, 1.
(20) Kreitz, S.; Penache, C.; Thomas, M.; Klages, C. P. *Surf. Coat. Technol.* **2005**, *200*, 676.
(21) Weller, R. A.; Ryle, W. T.; Newton, A. T.; McMahon, M. D.; Miller, T. M.; Magruder, R. H., III. *IEEE Trans. Nanotechnol.* **2003**, *2*, 154.
(22) Gray, J. E.; Norton, P. R.; Griffiths, K. *Thin Solid Films* **2005**, *484*, 196.
(23) Kordás, K.; Békési, J.; Bali, K.; Vajtai, R.; Nánai, L.; George, T. F.; Leppävuori, S. *J. Mater. Res.* **1999**, *14*, 3690.
(24) Byeon, J. H.; Park, J. H.; Yoon, K. Y.; Hwang, J. *Small*, in press.
(25) Weber, A. P.; Seipenbusch, M.; Kasper, G. *J. Phys. Chem. A* **2001**, *105*, 8958.
(26) Watters, R. L., Jr.; DeVoe, J. R.; Shen, F. H.; Small, J. A.; Marinenko, R. B. *Anal. Chem.* **1989**, *61*, 1826.
(27) Balazy, A.; Podgórski, A. *J. Colloid Interface Sci.* **2007**, *311*, 323.
(28) Byeon, J. H.; Park, J. H.; Yoon, K. Y.; Ko, B. J.; Ji, J. H.; Hwang, J. *Carbon* **2006**, *44*, 2106.
(29) Berkowitz, A. E.; Walter, J. L. *J. Mater. Res.* **1987**, *2*, 277.
(30) Persson, K.; Jansson, K.; Järås, S. G. *J. Catal.* **2007**, *245*, 401.
(31) Brunauer, S.; Emmett, P. H.; Teller, E. *J. Am. Chem. Soc.* **1938**, *60*, 309.